14th International Symposium on Turbulence and Shear Flow Phenomena (TSFP14)
Heidelberg, Germany, July 28–31, 2026

SUBCONVECTIVE WALL-SHEAR FLUCTUATIONS IN HIGH-REYNOLDS NUMBER BOUNDARY LAYERS

Tomek Jaroslawski, Jonathan Massey, Facundo Cabrera-Booman, and Beverley McKeon
Center for Turbulence Research
Stanford University
tomek@stanford.edu

Kyle Devlin and Alexander Smits
Department of Mechancial and Aerospace Engineering
Princeton University

ABSTRACT

Accurate prediction of wall-shear-stress (τ_w) fluctuations is critical for high-Reynolds-number (*Re*) skin-friction models, yet conventional methods fail by neglecting the influence of outer-scaling large-scale motions (LSMs). These LSMs impose a low-frequency, subconvective footprint on the wall. Subconvective structures, formally characterized by lower streamwise wavenumbers than the near-wall cycle, are understood to travel at phase velocities faster than near-wall values, and their spatial signature is measured in the temporal domain as low-frequency energy, with wavenumber and frequency related by the convective velocity. These dynamics were characterized using direct, time-resolved measurements of streamwise wall-shear-stress (τ_w) within a zero-pressure-gradient turbulent boundary layer, achieving an unprecedented friction Reynolds number of $Re_\tau \approx 10^4$. The resulting frequency spectra reveal a systematic amplification of this low-frequency, subconvective energy with increasing Reynolds number. Additionally, sensor spatial filtering effects were quantified using iso-*Re* experiments and filtered DNS data.

A data-driven model is proposed that decomposes the τ_w spectrum into a Reynolds-number-invariant, inner-scaled component (g_1) and a Reynolds-number-dependent, outer-scaled component (g_2). The model shows excellent agreement with experimental data, confirming that amplification of the outer component (g_2) accounts for the increased low-frequency energy originating from subconvective structures.

INTRODUCTION

In wall-bounded turbulence, wall-shear stress fluctuations are dominated by two primary sources: the small-scale motions of the near-wall cycle and the imprint of large- and very-large-scale motions (LSMs and VLSMs) from the inertial and outer layer. As Reynolds number increases, the relative importance of these outer-layer–induced, low-frequency contributions grows, altering spectra and scaling (Smits *et al.*, 2011).

Past studies have shown that the superposition of large-scale signatures on the wall region leaves a measurable imprint on τ_w (Metzger & Klewicki, 2001; Schlatter & Örlü, 2010; Mathis *et al.*, 2009, 2013). Specifically, low-frequency wall-shear stress fluctuations reflect the footprint of outer-layer motions, whose influence strengthens with Reynolds number (Deshpande *et al.*, 2025). These studies show that the high-frequency inner spectral peak preserves inner scaling, but the amplitude of the inner activity is modulated in time (and space) by outer-scaling large-scale motions. Thus, the wall footprint of these energetic outer structures superposes with near-wall activity, acting both as the source of low-frequency wall-shear-stress fluctuations and as the mechanism that amplitude-modulates the inner peak. These motions imprint directly on the wall, induce intermittency in skin friction, and complicate the development of predictive models and control strategies. Despite significant advances, the dynamics of low-frequency wall-shear-stress fluctuations remain insufficiently characterized, particularly at high Reynolds numbers, where their behavior departs from that observed in low-Re flows. Experimental data remain scarce, especially from direct unsteady measurements of τ_w, limiting our ability to fully assess their role.

In this paper, we employ unsteady wall-shear stress sensors to resolve the low-frequency content of τ_w across a range of Reynolds numbers. The measurements isolate the contribution of sub-convective motions to the wall-shear stress spectrum. These results underscore the importance of understanding the physical mechanisms for measurement limitations of wall-shear stress at high Reynolds number, as predictive models cannot be refined without accurately characterizing the underlying flow features.

EXPERIMENTS

Figure 1(a) presents a schematic of the pressurized wind tunnel, which was recently refurbished (De Graaff & Eaton, 2000; Cabrera-Booman *et al.*, 2024; Jaroslawski *et al.*, 2025). The facility attains high Reynolds numbers by enclosing the entire flow circuit within a pressure vessel and operating at elevated absolute pressure. Increasing the pressure raises the air density and reduces the value of the kinematic viscosity. This enables high Reynolds numbers (up to friction Reynolds numbers on the order of 10^4), defined as $Re_\tau \equiv u_\tau \delta / \nu$, where δ is the boundary layer thickness, u_τ is the friction velocity, and ν is the fluid's kinematic viscosity at modest development lengths, with thinner boundary layers and relatively low bulk velocities. Details of the tunnel geometry and ancillary systems are omitted here; we focus only on aspects relevant to the current experiment. For further information, the reader is referred to De Graaff & Eaton (2000).

The working section measures 3.0 × 0.15 × 0.71 m (length × height × width). The lower wall incorporates a removable transparent plate with an inset region (0.95 × 0.30 m) accommodating a 6-mm-thick aluminum plate flush-mounted to the wall. Precision-drilled holes and associated flush-mounted insets/plugs in the inset plate allow for flush-mounted pressure and shear-stress instrumentation (Figure 1(b)). The upstream step height at the leading edge of the inset was measured to be less than 200 μm under atmospheric conditions, and measurement stations were placed more than 2,500 step heights downstream to eliminate any influence of the step. Freestream velocity, U_e, was determined using a static-pressure Pitot tube connected to a manometer, positioned approximately at midchannel 2.6 m downstream of the trip. The facility provided stable freestream velocities in the range of 3–14 m/s, with the air density variable from atmospheric (1.2 kg/m^3) to a maximum of 9.5 kg/m^3. This combination of parameters enabled access to a friction Reynolds number (Re_τ) range extending from approximately 500 to 9000

Characterisation of the incident flat-plate boundary layer was performed on the wind tunnel floor using hot-wire anemometry. Although the data are not presented herein for the sake of of brevity, the resulting velocity profiles demonstrated agreement with the canonical data of De Graaff & Eaton (2000). The constant cross-section of the test section induces a slightly favourable pressure gradient due to boundary-layer growth; however, the associated acceleration parameter, $K = (\nu/U_e^2)(dU_e/dx)$, is known to be $K \ll 1 \times 10^{-6}$ for this facility. Consequently, the effects of flow acceleration are deemed to be insignificant. This is corroborated by the observation that the measured velocity profiles show no discernible deviation from the established logarithmic law of the wall.

The streamwise component of the wall-shear stress, τ_w, was measured using flush-mounted capacitive sensors (IC2 CS-0510) located on the spanwise centerline approximately 2.5 m downstream of the trip. Sensors were installed to tight tolerances, with a maximum step between the sensing surface and the wall of 25 μm; the manufacturer specifies $<$25 μm on the sensitive element itself, which at the highest Reynolds numbers corresponds to about 5 viscous units ($y^+ \equiv y u_\tau/\nu$). Each sensing element has a 2.0 × 0.4 mm footprint, implying finite spatial averaging at the wall. The usable bandwidth is approximately 700 Hz (due to sensor resonance). Signals were sampled at 5 kHz with an analog low-pass filter at 700 Hz. Acquisition durations spanned many eddy turnover times to ensure statistical convergence.

MODEL

A semi-analytical model for the frequency spectrum of wall-shear-stress fluctuations, $\Phi_{\tau\tau}$, is proposed. The model framework builds on the idea that near-wall turbulence may be decomposed into inner- and outer-scaled contributions, in the spirit of Townsend's active/inactive picture of wall turbulence (Townsend, 1961; Bradshaw, 1967; Morrison, 2007). Gustenyov *et al.* (2025) made this explicit in a successful model for the power spectrum of the streamwise velocity, and Massey *et al.* (2025) recently applied the same approach to the pressure spectrum. Following this framework, the wall-shear-stress spectrum is represented as a linear superposition of two distinct contributions associated with inner- and outer-scaled motions:

$$\Phi_{\tau\tau} = g_1(T^+) + g_2(T^o; Re_\tau) \qquad (1)$$

The first component of the model, denoted g_1, accounts for the turbulent fluctuations at small scales, which are characteristic of the boundary layer's inner region. This component is modeled using a log-normal distribution with respect to the inner-scaled temporal period, T^+. The period T^+ is non-dimensionalized using inner-wall variables and is defined as the reciprocal of the inner-scaled frequency, f^+: $T^+ = \frac{1}{f^+}$ where $f^+ = \frac{f\nu}{u_\tau^2}$. Here, f is the dimensional frequency. We assume a functional form for g_1:

$$g_1(T^+) = 0.054 r_v \exp\left\{-1.4\left[\log\left(\frac{T^+}{90}\right)\right]^2\right\} \qquad (2)$$

where r_v is a coefficient accounting for viscous damping effects near the wall.

The second component, g_2, captures the signature of the large-scale, energy-containing motions from the outer region of the boundary layer. This contribution is dependent on the friction Reynolds number, Re_τ, and the outer-scaled period, T^{o}:

$$g_2(T^o; Re_\tau) = 0.0046(\log Re_\tau - 2.6)\exp\left[-0.37\log^2(T^{\mathrm{o}})\right] \qquad (3)$$

Here, the outer-scaled period is defined as $T^{\mathrm{o}} = TU_e/\delta$. The combined model, therefore, is capable of capturing the bimodal nature of the wall-shear-stress spectrum across a range of Reynolds numbers.

The model forms were synthesized from a combination of sources covering a wide range of Reynolds numbers. These include: (1) low-Reynolds-number DNS data (Eitel-Amor *et al.*, 2014); (2) moderate-Reynolds-number models from experimental data (Mathis *et al.*, 2013); and (3) high-Reynolds-number surface layer data (Marusic & Heuer, 2007).

RESULTS

Mean skin friction versus Reynolds number

Figure 2 presents the mean skin-friction coefficient, C_f, as a function of the friction Reynolds number, Re_τ, derived from our direct measurements of wall-shear stress. Data span a range of speeds and freestream (tank) pressures. For reference, the plot includes a spread of empirical correlations in the literature (namely, the 1/4- and 1/7-power laws) alongside results from De Graaff & Eaton (2000), in which the wall-shear stress, τ_w, was inferred by least-squares fitting of the logarithmic law to the mean velocity profile over the interval $50 \leq y^+$ and $y/\delta \leq 0.2$. The present measurements are consistent with De Graaff & Eaton (2000) within the stated experimental uncertainty and reproduce the same trend.

The relatively large uncertainties observed at low Reynolds numbers are anticipated. Under low freestream pressure, the physical wall-shear forces are small, placing the shear-stress sensor near the lower end of its dynamic range. In this regime, resolution and broadband noise constitute a larger

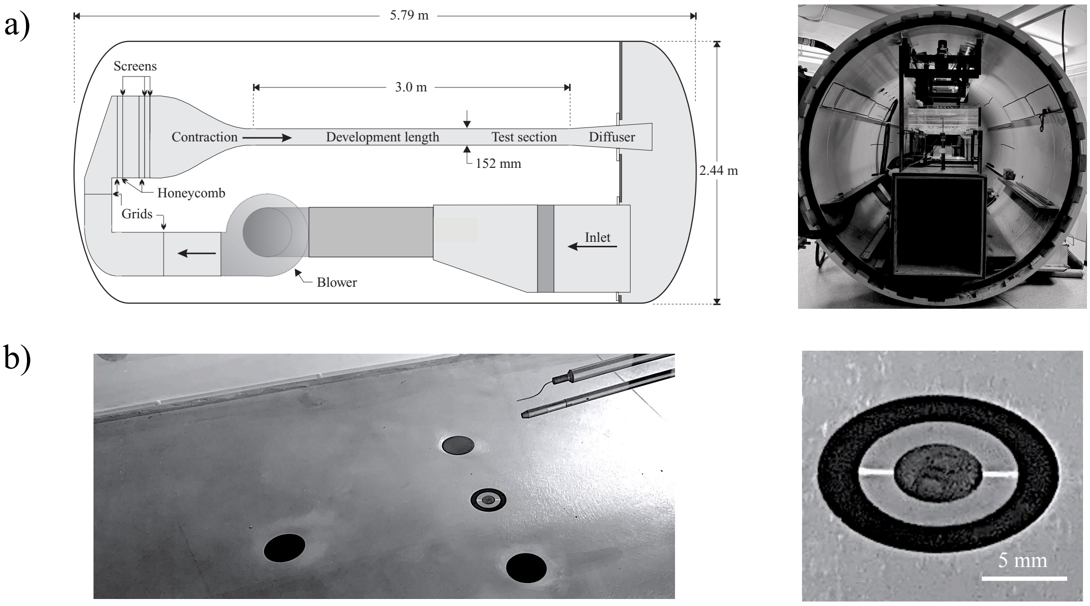

Figure 1. (a) Schematic (adapted from De Graaff & Eaton, 2000) (left) and photograph of the facility with the test-section door open (right). (b) Inset of the test section (left) and close-up view of the wall-shear-stress sensor (right).

fraction of the signal, and temperature-induced offset drift is less effectively suppressed, which degrades the signal-to-noise ratio. Consequently, the relative uncertainty in τ_w—and, by propagation, in C_f—is elevated at low Re_τ.

Spectral content of τ_w': Iso-Reynolds-number experiments

Here we present wall-shear-stress spectra at iso-Reynolds numbers. The Reynolds number is controlled by adjusting freestream velocity U_e and pressure (hence density ρ) at near-constant temperature; for iso-Reynolds-number operation, U_e and ρ are covaried to keep Re_τ constant. Increasing pressure raises ρ and lowers $\nu = \mu/\rho$. As the viscous length scale is a function of ν, this control strategy directly impacts the sensor's non-dimensional size. The resulting streamwise (l_x^+) and spanwise (l_z^+) dimensions are summarized in Table 1.

Figure 3 shows the premultiplied wall-shear-stress spectrum, $f\phi^+_{\tau_w\tau_w}$, plotted against the inner-scaled period, T^+. We compare two friction Reynolds numbers, $Re_\tau \approx 1200$ and $Re_\tau \approx 6000$, and include DNS data from Eitel-Amor *et al.* (2014) for reference. The $Re_\tau \approx 1200$ condition was reproduced under iso-Re_τ conditions by reducing the freestream velocity while increasing the test-section pressure, yielding the same Re_τ as at atmospheric pressure with $U_e \approx 14$ m/s.

Two features emerge. First, the spectral energy attenuates at $T^+ < 1000$, attributable to spatial averaging by the finite-sensing element ($\sim$0.4 mm), which increasingly under resolves the shrinking viscous scales. Second, the spectra collapse at large T^+ (low frequencies) across all iso-Re_τ realizations, consistent with DNS and indicating that spatial filtering does not contaminate the larger timescales to the first order. At $Re_\tau \approx 6000$, we observe similar attenuation due to spatial filtering for $T^+ < 100$. At large T^+, the spectra again collapse and exhibit more energy than the low-*Re* DNS reference; this topic is discussed in the next section.

Table 1. Effective sensor dimensions in the streamwise (l_x^+) and spanwise (l_z^+) directions, normalized by the viscous length scale, δ_ν. The viscous scaling is determined from the measured mean streamwise wall-shear stress ($\overline{\tau_w}$).

Re_τ	$\delta_\nu (\mu\text{m})$	l_x^+	l_z^+
1200	26	77	15
	23	87	17
	21	95	19
6000	5.9	339	68
	5.4	370	74
	5.0	400	80

Synthetic assessment of spatial attenuation by finite sensor footprint

Understanding the limitations of the shear sensor is vital for interpreting the results. We therefore synthetically model the effect of an increasing inner-scaled sensor footprint using DNS of turbulent channel flow at $Re_\tau \approx 550$. The objective is to isolate the impact of spatial averaging on the measured wall-shear spectra when the sensor dimensions are fixed in outer units, so that ℓ^+ increases linearly with Re_τ.

The DNS provides instantaneous wall-shear fields on both walls, $\tau_w(x,z,t)$, reconstructed from the stored wall-normal velocity gradient via $\tau_w = \nu(\partial u/\partial y)_w$ (with $\rho = 1$). The sensor is modelled as a rectangular spatial average,

$$\tau_w^{(s)}(x_0,z_0,t) = \iint h(\Delta x,\Delta z)\, \tau_w(x_0-\Delta x,\, z_0-\Delta z,\, t)\, \mathrm{d}\Delta x\, \mathrm{d}\Delta z, \tag{4}$$

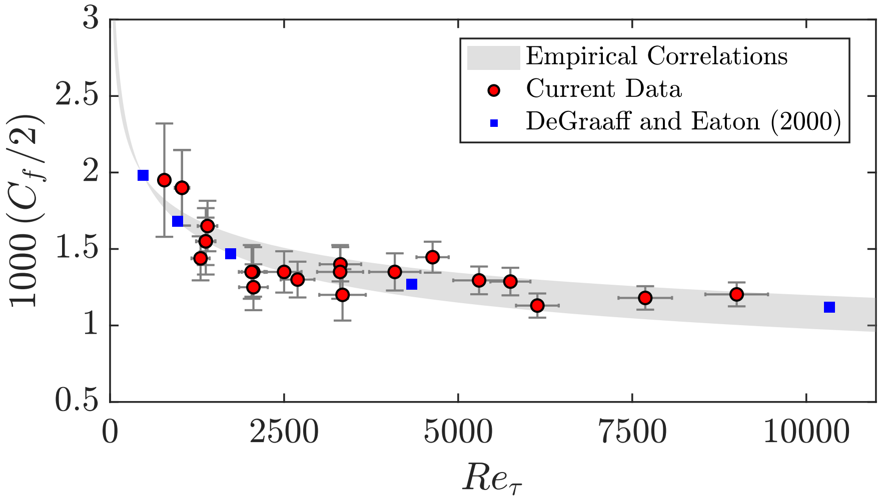

Figure 2. Mean skin-friction coefficient versus the friction Reynolds number. Experimental results are plotted across a range of speeds and freestream pressures.

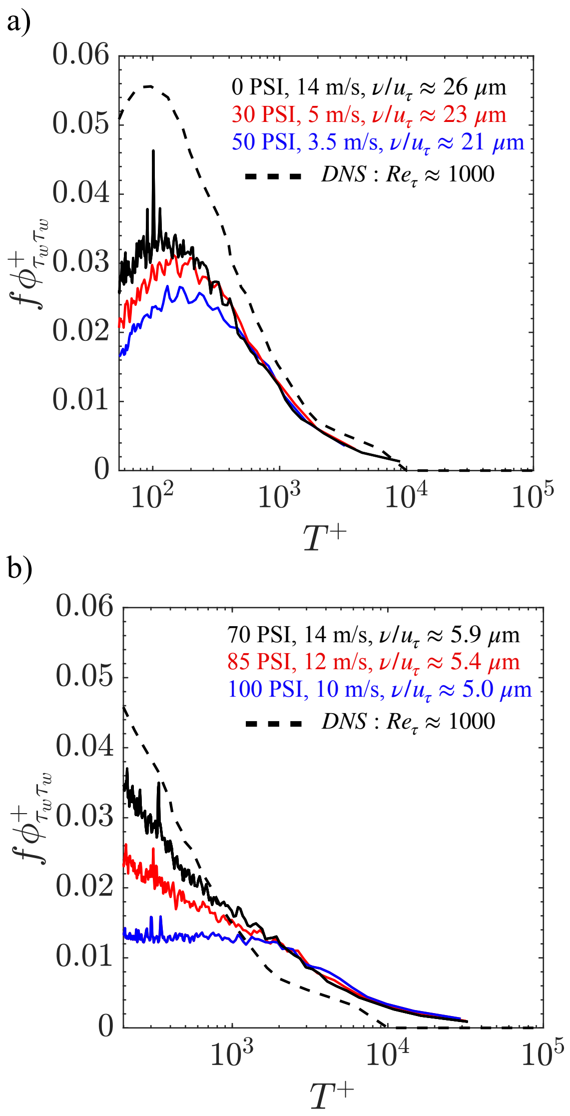

Figure 3. Iso-Reynolds-number experiments obtained under three different freestream conditions. (a) $Re_\tau \approx 1200$. (b) $Re_\tau \approx 6000$. The dashed line represents data obtained from Eitel-Amor *et al.* (2014).

with a top-hat kernel

$$h(\Delta x, \Delta z) = \begin{cases} (\ell_x \ell_z)^{-1}, & |\Delta x| \le \ell_x/2 \text{ and } |\Delta z| \le \ell_z/2, \\ 0, & \text{otherwise,} \end{cases} \quad (5)$$

where ℓ_x and ℓ_z are the streamwise and spanwise dimensions of the active area. For the experiment, the planform dimensions are fixed in physical units, hence the inner-scaled footprint increases with Reynolds number according to

$$\ell_x^+ = \frac{u_\tau \ell_x}{\nu} = Re_\tau \frac{\ell_x}{\delta}, \qquad \ell_z^+ = \frac{u_\tau \ell_z}{\nu} = Re_\tau \frac{\ell_z}{\delta}, \quad (6)$$

Using the experimental geometry ($\ell_x = 2$ mm, $\ell_z = 0.4$ mm, $\delta \approx 35$ mm).

Figure 4a compares the unfiltered wall shear stress time series from DNS with the signal filtered to simulate a sensor's spatial footprint. The filtered signal qualitatively exhibits an attenuation of high-frequency content. This effect is quantified in Figure 4b, which presents the premultiplied power spectral density of the wall shear stress fluctuations for both signals. Consistent with experimental data at comparable Reynolds numbers, the spectral energy of the filtered signal attenuates at high frequencies. This finding corroborates the hypothesis from the preceding section: the attenuation is attributable to spatial averaging by the finite-sensing element (~0.4 mm), which increasingly under-resolves the shrinking viscous scales.

Spectral content of τ_w': effects of Re_τ

This section presents experimental measurements of wall shear stress fluctuations and compares them with model predictions. Figure 5 displays the premultiplied spectra of wall-shear-stress fluctuations over a friction Reynolds number range of $Re_\tau \approx 1500$ to 9000. The experimental data reveal two primary trends as Re_τ increases. First, there is a systematic rise in spectral energy at large temporal periods, indicating a strengthening of low-frequency fluctuations. This is attributed to the growing influence of large-scale outer-layer motions, whose subconvective signatures create long-period events in the wall-shear signal (Metzger & Klewicki, 2001; Mathis *et al.*, 2013;

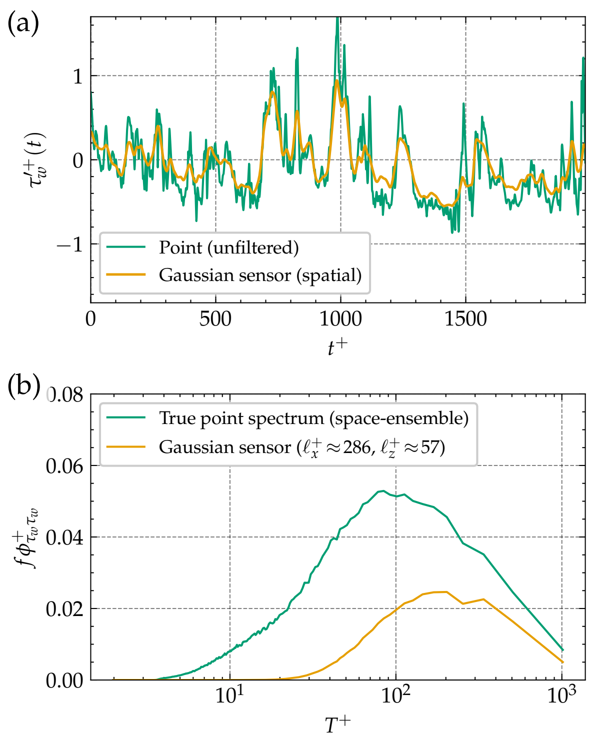

Figure 4. Emulation of a finite-sized sensor's spatial filtering effect. a) Comparison of the unfiltered and spatially filtered wall-shear stress time series. b) Comparison of premultiplied power spectra for the unfiltered and spatially filtered wall-shear stress signals

Deshpande *et al.*, 2025). Second, consistent with the analysis in the previous sections, the spectra show attenuation at short temporal periods due to the sensor's spatial filtering.

Referring to Figure 5, the model predictions are overlaid on the experimental data. The total model output (solid lines) is decomposed into two components: the inner-layer contribution, g_1 (dashed lines), and the outer-layer contribution, g_2 (dotted lines). Overall, the model shows agreement with the experimental measurements, particularly in the energetic region of interest that is unaffected by the sensor's filtering limitations (unshaded region).

CONCLUSIONS

In this work, we presented direct, time-resolved measurements of wall-shear-stress fluctuations in a high-Reynolds-number turbulent boundary layer, spanning from $Re_\tau \approx 1500$ to 9000. A key challenge in these experiments is the spatial filtering imposed by the sensor's finite physical size. Through a combination of iso-Reynolds-number experiments and synthetic filtering of DNS data, we systematically quantified this effect. Our analysis confirms that the sensor attenuates high-frequency spectral content corresponding to the small viscous scales, but critically, it leaves the low-frequency energy associated with larger turbulent structures largely unaffected. The validated low-frequency data revealed a systematic and significant growth in spectral energy with increasing Reynolds number. This trend is a direct signature of the intensified influence of large-scale, energy-containing motions from the outer layer on the near-wall flow. To explain this behavior, we proposed and validated a semi-analytical spectral model. The model's key innovation is the decomposition of the wall-shear-stress spectrum into two components: a Reynolds-number-invariant inner contribution (g_1) and a Reynolds-number-dependent outer contribution (g_2). The model successfully captures the experimental trends, demonstrating that the growth of the g_2 term quantitatively reproduces the observed rise in low-frequency energy. This provides strong evidence that the high Reynolds number scaling of wall-shear-stress fluctuations is driven almost entirely by the increasing footprint of the outer-layer motions.

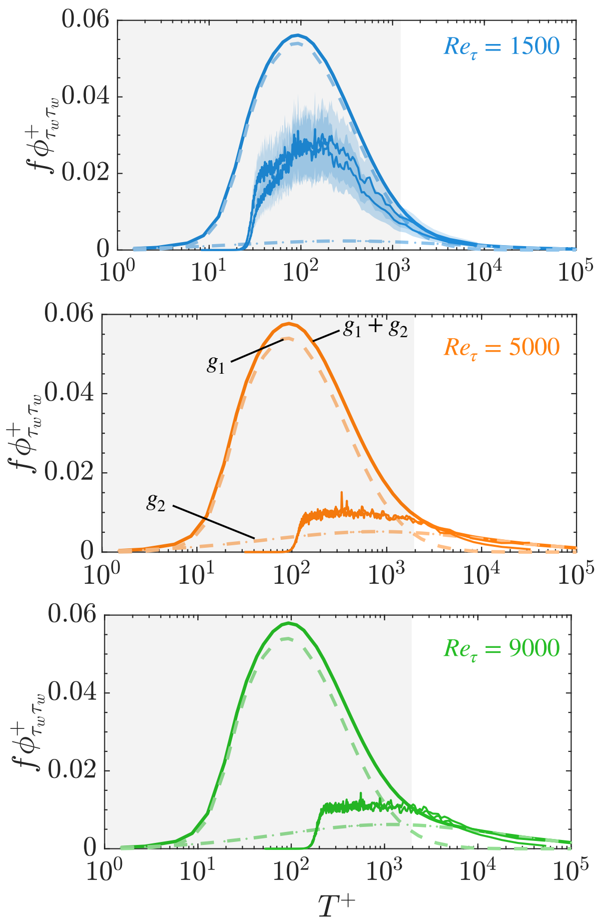

Figure 5. Effect of Reynolds number on the premultiplied spectra of wall-shear stress fluctuations. Experimental data at $Re_\tau \approx 1500$, 5000, and 9000 are shown alongside overlaid model predictions for comparison.

ACKNOWLEDGMENTS

The support of DARPA under the award of HR0011-24-9-0465 is gratefully acknowledged.

REFERENCES

Bradshaw, P. 1967 'Inactive' motion and pressure fluctuations in turbulent boundary layers. *Journal of Fluid Mechanics* **30**, 241–258.

Cabrera-Booman, Facundo, Massey, Jonathan MO & McKeon, Beverley J 2024 High-Reynolds-number and low-Mach-number wind tunnel at Stanford University .

De Graaff, David B & Eaton, John K 2000 Reynolds-number scaling of the flat-plate turbulent boundary layer. *Journal of Fluid Mechanics* **422**, 319–346.

Deshpande, Rahul, Vinuesa, Ricardo, Klewicki, Joseph & Marusic, Ivan 2025 Active and inactive contributions to the wall pressure and wall-shear stress in turbulent boundary layers. *Journal of Fluid Mechanics* **1003**, A24.

Eitel-Amor, Georg, Örlü, Ramis & Schlatter, Philipp 2014 Simulation and validation of a spatially evolving turbulent boundary layer up to Re_θ= 8300. *International Journal of Heat and Fluid Flow* **47**, 57–69.

Gustenyov, Nikolay, Bailey, Sean CC & Smits, Alexander J 2025 A model spectrum for turbulent wall-bounded flow. *Journal of Fluid Mechanics* **1016**, A23.

Jaroslawski, Tomek M, Cabrera-Booman, Facundo, Massey, Jonathan MO & McKeon, Beverley J 2025 Wall-shear-stress measurement and characterization at high Reynolds numbers .

Marusic, Ivan & Heuer, Weston DC 2007 Reynolds number invariance of the structure inclination angle in wall turbulence. *Physical Review Letters* **99** (11), 114504.

Massey, Jonathan M. O., Smits, Alexander J. & McKeon, Beverley J. 2025 Eddy population based model for the wall-pressure spectrum at high Reynolds number. *Journal of Fluid Mechanics, to appear, and arXiv preprint arXiv:2507.23098* .

Mathis, Romain, Hutchins, Nicholas & Marusic, Ivan 2009 Large-scale amplitude modulation of the small-scale structures in turbulent boundary layers. *Journal of Fluid Mechanics* **628**, 311–337.

Mathis, Romain, Marusic, Ivan, Chernyshenko, Sergei I & Hutchins, Nicholas 2013 Estimating wall-shear-stress fluctuations given an outer region input. *Journal of Fluid Mechanics* **715**, 163–180.

Metzger, MM & Klewicki, JC 2001 A comparative study of near-wall turbulence in high and low Reynolds number boundary layers. *Physics of Fluids* **13** (3), 692–701.

Morrison, Jonathan F. 2007 The interaction between inner and outer regions of turbulent wall-bounded flow. *Philosophical Transactions: Mathematical, Physical and Engineering Sciences* **365** (1852), 683–698.

Schlatter, Philipp & Örlü, Ramis 2010 Assessment of direct numerical simulation data of turbulent boundary layers. *Journal of Fluid Mechanics* **659**, 116–126.

Smits, Alexander J, McKeon, Beverley J & Marusic, Ivan 2011 High–Reynolds number wall turbulence. *Annual Review of Fluid Mechanics* **43** (1), 353–375.

Townsend, A. A. 1961 Equilibrium layers and wall turbulence. *Journal of Fluid Mechanics* **11** (1), 97–120.